Electronic Supplementary Information (ESI)

Self-templated synthesis of uniform nanoporous $CuCo_2O_4$ double-shelled hollow spheres for high-performance asymmetric supercapacitors

Saeid Kamari Kaverlavani[a], Seyyed Ebrahim Moosavifard[b*] and Ali Bakouei[a*]

[a]Department of Physics, Tarbiat Modares University, Tehran, Iran. Email: a.bakouei@modares.ac.ir.
[b]Young Researchers and Elite Club, Central Tehran Branch, Islamic Azad University, Tehran, Iran. Email: info_seyyed@yahoo.com; Tel/Fax: +98 21 66612673.

Experimental details

Synthesis of the multilevel interior nanoporous $CuCo_2O_4$ microspheres:

The multilevel interior nanoporous $CuCo_2O_4$ microspheres were synthesized by a facile self-templated method. In a typical synthesis, 36.95 mg of $Cu(NO_3)_2{\cdot}6H_2O$, 72.75 mg of $Co(NO_3)_2{\cdot}6H_2O$, and 8 mL of glycerol were added to 40 mL isopropanol under stirring to obtain a homogeneous apparent solution. The result pink solution was then transferred into a sealed Teflon-lined stainless-steel autoclave and maintained at 180 °C for 6 h. After cooling down to room temperature, the as-synthesized CuCo-glycerate precursor was washed with ethanol and dried in at 80 °C. In order to obtain the multilevel interior nanoporous $CuCo_2O_4$ microspheres, the as-synthesized CuCo-glycerate precursors were then annealed at 350 °C in air for 2 h with a different heating rate of 1, 2, 4 and 10 °C min^{-1}. The bulk sample was synthesized by the above procedure without addition of glycerol, and with a heating rate of 1 °C min^{-1}.

Characterization

Structurally characterizations were performed using X-ray powder diffraction (XRD, Philips X'pert diffractometer with Co K_α radiation (λ = 0.178 nm) generated at 40 kV and 30 mA with a step size of 0.04° s^{-1}). X-ray photoelectron spectroscopy (XPS) analyze was conducted on a VG ESCALAB MKII spectrometer using an Mg K_α X-ray source (1253.6 eV, 120 W) at a constant analyzer. Nitrogen adsorption/desorption, specific surface area and pore size distributions were carried out using a Micromeritics ASAP-2010 apparatus at 77 K. The morphologies and structural investigations were done by a Zeiss field-emission scanning electron microscope (FESEM) and a Philips EM 208 transmission electron microscope (TEM). Electrochemical measurements were performed on a BioLogic VSP 300 potentiostat/galvanostat device.

Electrochemical measurements

All electrochemical measurements were performed in aqueous 3 M KOH solution as the electrolyte. The electrodes were prepared by mixing active material, acetylene black, and polyvinylidene fluoride (PVDF) with a mass ratio of 85:10:5. A 10% solution of the mixture in acetone was prepared and coated on nickel foam as the current collector by a coater (3Z-M. T. D. I. 900, Modern Technology Development Institute,

Iran) and then dried in 120 ◦C for 2 h. In three-electrode cell configuration, the as-prepared electrodes were used as the working electrode, while an Hg/HgO electrode and a platinum foil were used as the reference and counter electrodes, respectively. In two-electrode cell configuration (asymmetric device), the as-prepared DS-CCO and AC electrodes were used as the positive and negative electrodes, respectively. For the preparation of the AC electrode, a mixture of the AC powder, carbon black and polytetrafluoroethylene (PTFE) in the weight ratio 85:10:5 was pressed onto a nickel foam and dried at 120 °C for 2 h. According to the specific capacitance of AC electrode (183 F g^{-1}), and in order to achieve the maximum operating potential window and performance, the optimal mass ratio between the positive and negative electrodes (m^+/m^-) was calculated to be around 0.249 based on the charge balance theory ($q^+ = q^-$). So, the total mass of the two electrode materials was 10 mg cm^{-2}.

The specific capacitances (C_{sp}), energy densities (ED, Wh kg^{-1}) and power densities (PD, W kg^{-1}) were calculated from the discharge curves using the following equations:

$$C_{sp} = \frac{I\Delta t}{m\Delta V} \quad (1)$$

$$ED = \frac{C_{sp}\Delta V^2}{2} \quad (2)$$

$$PD = \frac{ED}{\Delta t} \quad (3)$$

where I is the discharge current (A), Δt is the discharge time (s), ΔV is the potential window (V), and m is the mass loading (g).

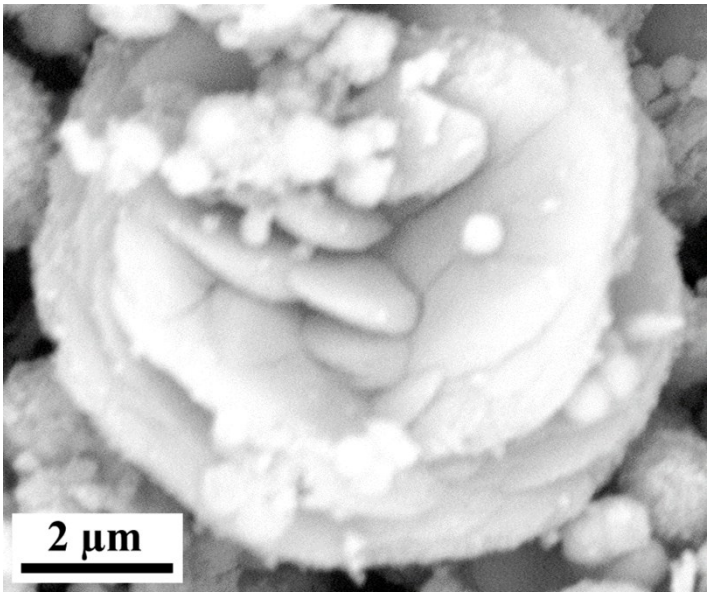

Fig. S1 FESEM image of the as-synthesized bulk sample.

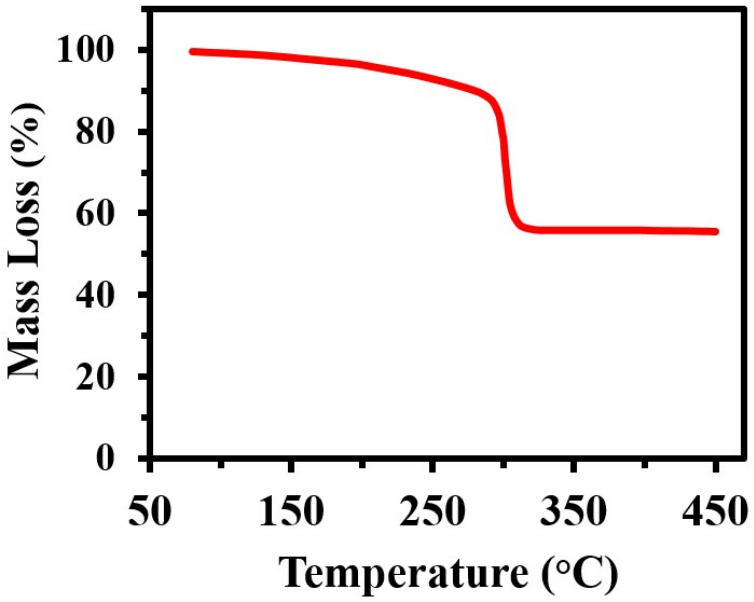

Fig. S2 Thermal gravimetric analysis (TGA) of CuCo-glycerate precursor microspheres with a temperature ramp of 10 °C min^{-1} under air flow.

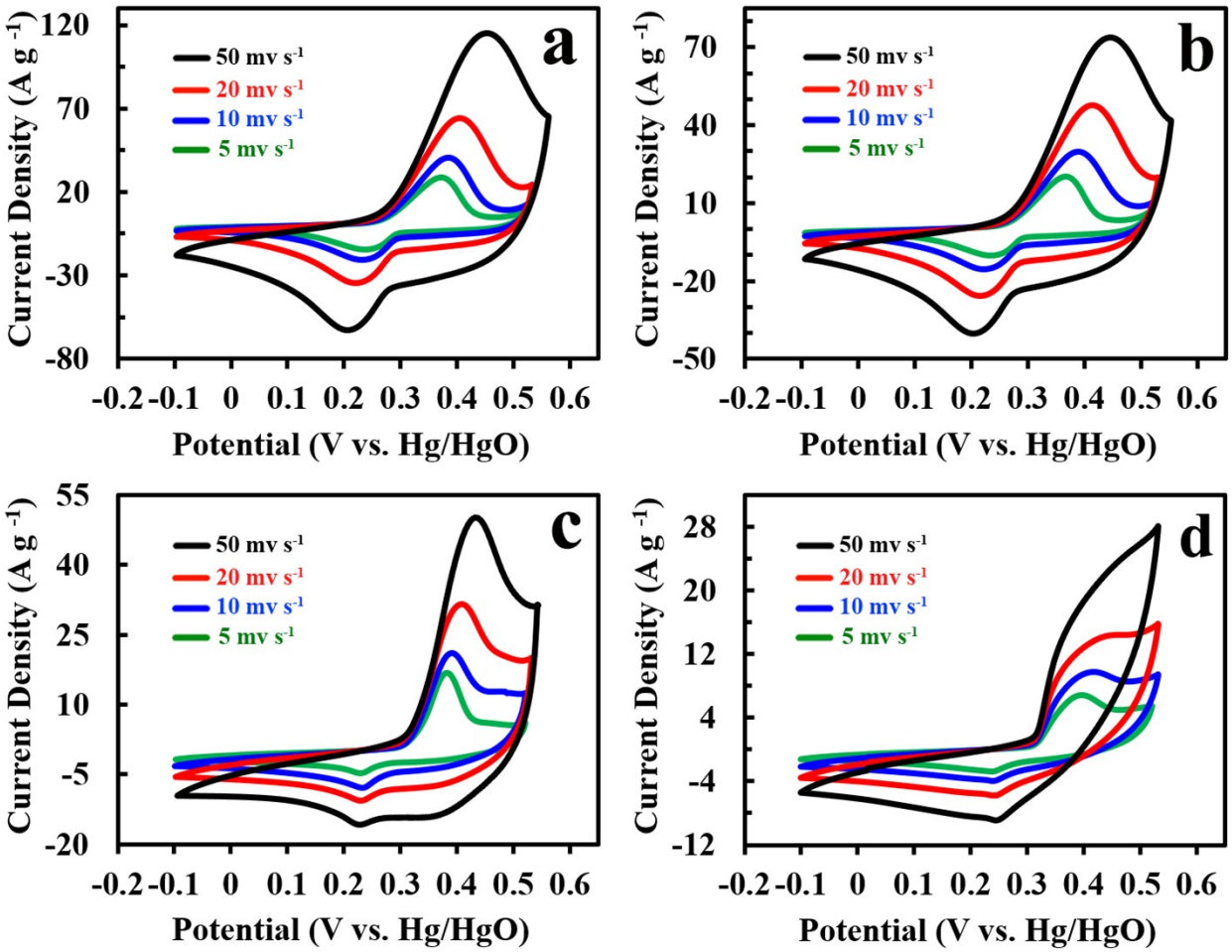

Fig. S3 CV curves of the as-prepared (a) single-shell hollow microspheres, (b) core-shell microspheres, (c) solid microspheres and (d) bulk $CuCo_2O_4$ electrodes in aqueous 3 M KOH electrolyte at a various scan rates ranged from of 5 to 50 mV s^{-1}.

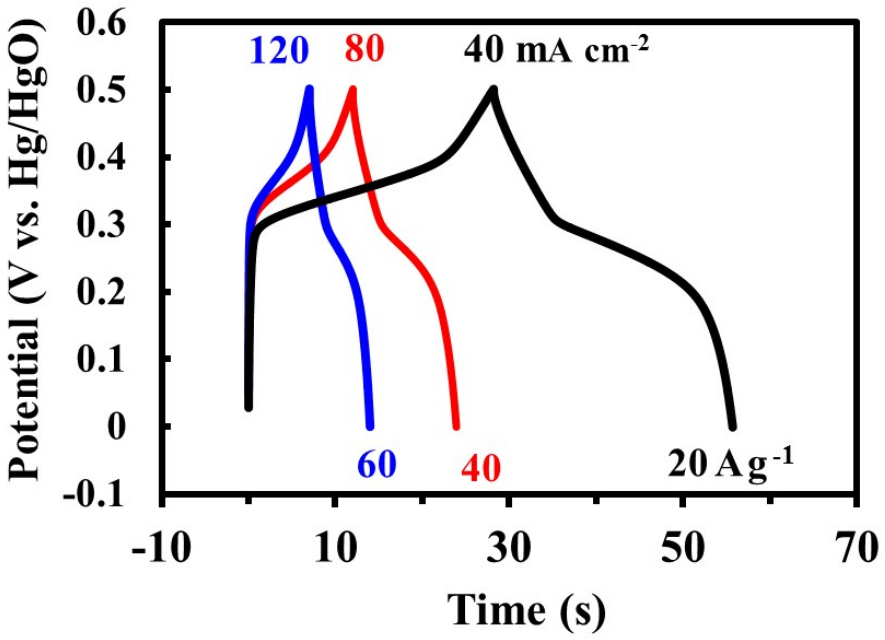

Fig. S4 CD curves of the double-shell $CuCo_2O_4$ hollow microspheres electrode at high current densities ranged from 40 to 120 mA cm^{-2}.

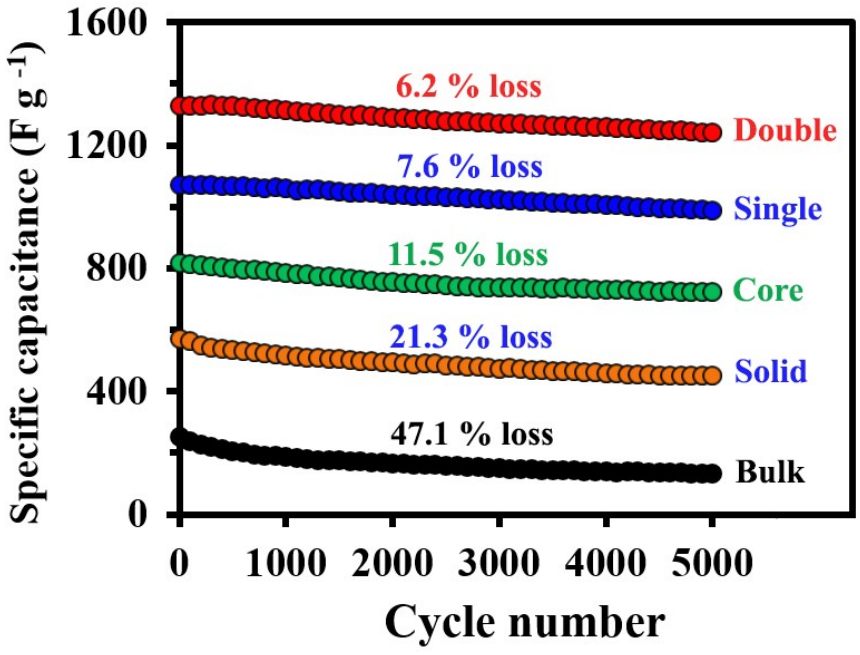

Fig. S5 Long-term cycling stability of the as-prepared electrodes over 5000 continuous CDs at a current density of 10 mA cm^{-2} in three-electrode system.

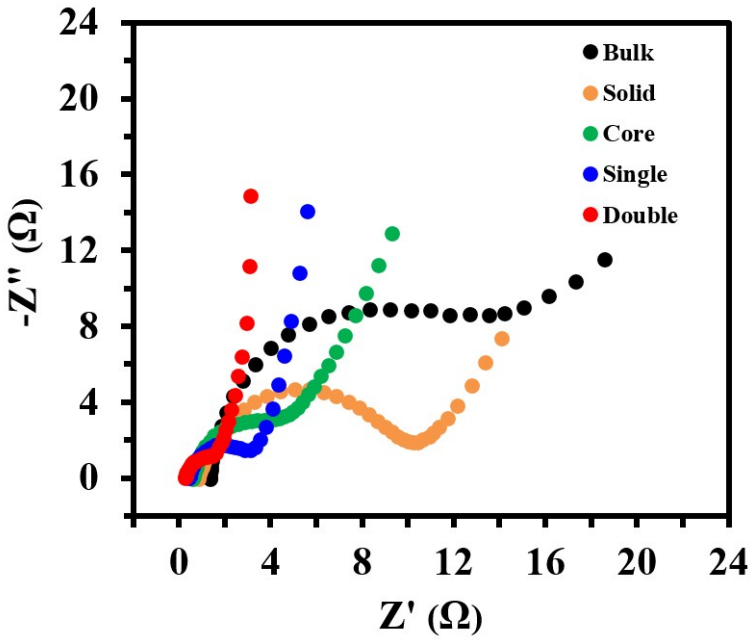

Fig. S6 EIS plot of the as-prepared electrodes. In order to further electrochemical investigation of the electrodes, EIS experiments were performed. The depressed semicircle at the high frequency region corresponds to charge transfer resistance (R_{ct}) caused by Faradaic reactions. The straight line in the medium frequency region ascribed to Warburg impedance (Z_w) relates to the diffusion resistance of electrolyte ions within the nanostructures. The steeper line at low frequencies demonstrates the capacitive nature of the electrode (vertical line for an ideal capacitor). Obviously, the double-shelled $CuCo_2O_4$ electrode exhibits a lowest R_{ct}, lowest internal resistance (R_b) and a more vertical line at low frequencies, indicating a highest electron/ion conductivity and a largest electro-active surface area.

Table S1. Comparison of the electrochemical performance of as-prepared electrodes in three-electrode system.

Morphology	Max capacitance	Min capacitance	Rate capability	Cycling stability after 5000 cycles
Double-shell hollow spheres	1472 A g^{-1} 2.94 mA cm^{-2}	837 A g^{-1} 1.67 mA cm^{-2}	57 %	6.2 % loss
Single-shell hollow spheres	1216 A g^{-1} 2.43 mA cm^{-2}	609 A g^{-1} 1.22 mA cm^{-2}	50 %	7.6 % loss
Core-shell spheres	943 A g^{-1} 1.89 mA cm^{-2}	412 A g^{-1} 0.82 mA cm^{-2}	44 %	11.5 % loss
Solid spheres	664 A g^{-1} 1.33 mA cm^{-2}	235 A g^{-1} 0.47 mA cm^{-2}	35 %	21.3 % loss
Bulk	306 A g^{-1} 0.61 mA cm^{-2}	70 A g^{-1} 0.14 mA cm^{-2}	23 %	47.1 % loss

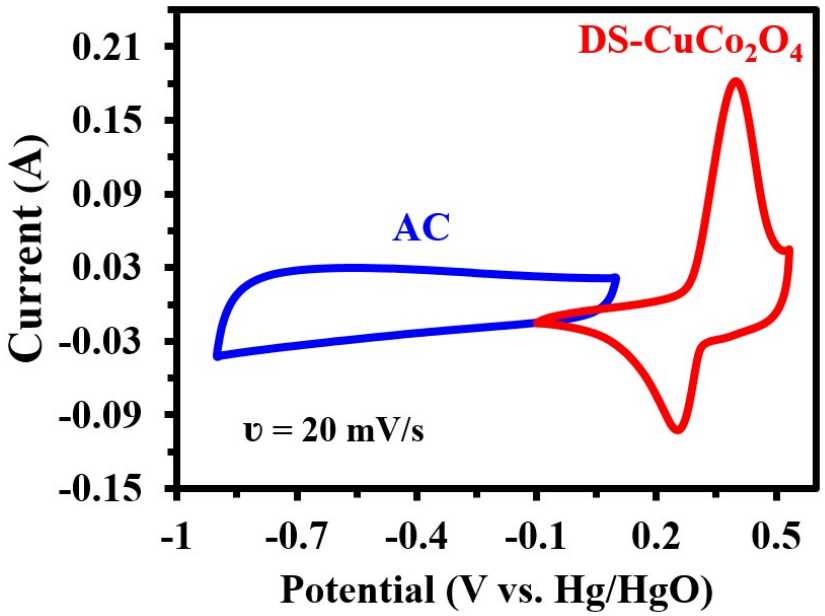

Fig. S7 CV curves of charge-balanced DS-$CuCo_2O_4$ and AC electrodes at a scan rate of 20 mV s^{-1} in a three-electrode system.

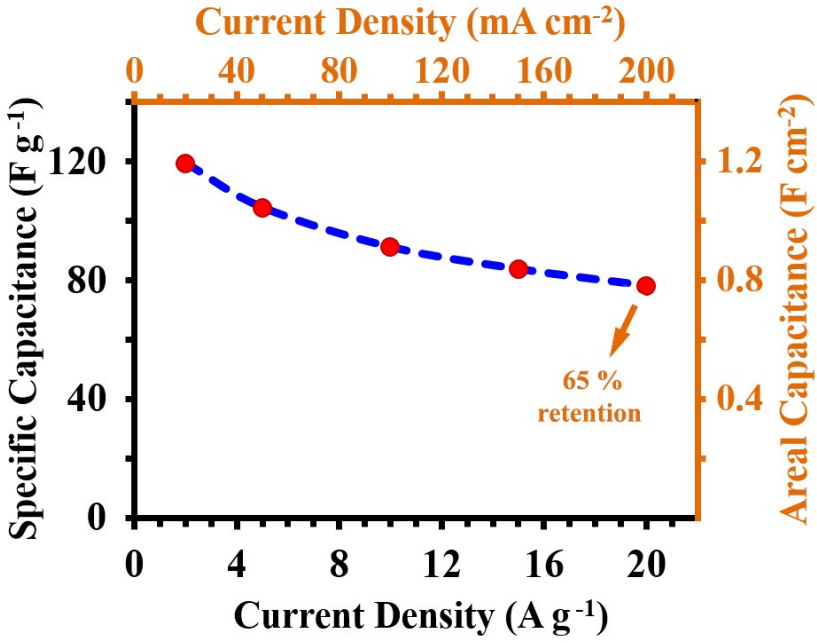

Fig. S8 The rate capability of the as-prepared DS-CCO//AC asymmetric supercapacitor device at various current densities.

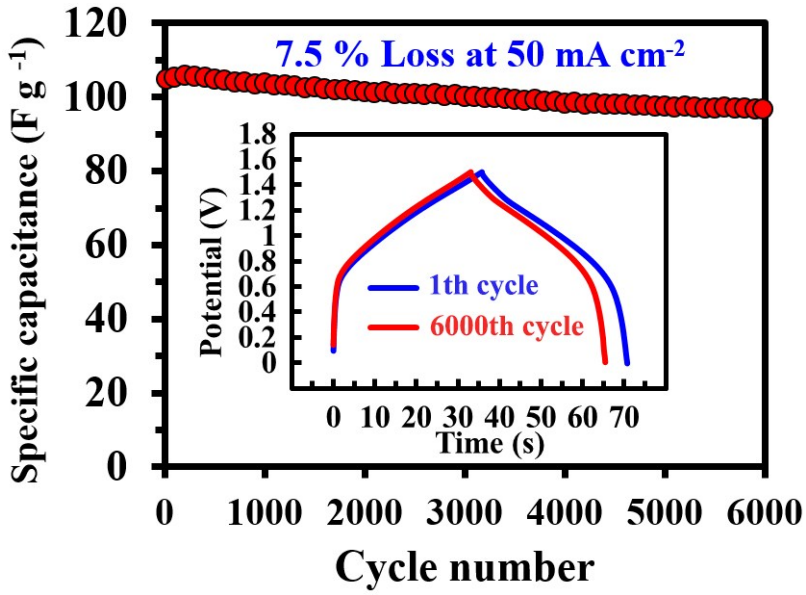

Fig. S9 Long-term cycling stability of the as-prepared DS-CCO//AC device over 6000 continuous CDs at a current density of 50 mA cm^{-2}.

Table S2. Comparison of the electrochemical performance of DS-CCO electrode in three- and two-electrode systems with other previously reported electrodes.

Morphology/Composition	Capacitance @current density	Cell (Config)	Cycles	Retention	ED (Wh/kg)	Electrolyte	ΔV (V)	Reference (year)
$CuCo_2O_4$ nanowires	0.44 F/cm² at 1 mA/cm²	3E	1500	90% at 1 mA/cm²	-	KOH	0.45	S1(2015)
	0.47 F/cm² at 10 mV/s	2E (vs. AC)	3000	82% at 2 mA/cm²	-	KOH	1.5	
$CuCo_2O_4$ nanograsses	796 F/g at 2 A/g	3E	5000	94.7% at 2 A/g	-	KOH	0.6	S2(2015)
$CuCo_2O_4$ nanobelts	809 F/g at 10 mV/s	3E	1800	127% at 26 mA/cm²	-	KOH	0.45	S3(2015)
$CuCo_2O_4$ @MnO_2 nanoflakes	416 F/g at 1 A/g	3E	4200	92% at 8 A/g	-	Na_2SO_4	1	S4(2015)
	78 F/g at 1 A/g	2E (vs. AG)	-	-	43.3	Na_2SO_4	2	
$CuCo_2O_4$ @MnO_2 on carbon fibers	327 F/g at 1.25 A/g	3E	5000	90% at 6.25 A/g	-	KOH	0.5	S5(2014)
	0.71 F/cm² at 1 mA/cm²	2E (Symm)	-	-	-	PVA/KOH	1	
$CuCo_2O_4$ nanowire @$NiCo_2O_4$ nanosheet	2.6 F/cm² at 10 mA/cm²	3E	4500	80% at 10 mA/cm²	-	KOH	0.42	S6 (2015)
$CuCo_2O_4$/$MnCo_2O_4$ on graphite paper	1434 F/g at 0.5 A/g	3E	5000	81.4% at 10 A/g	-	KOH	0.5	S7 (2016)
	118.4 F/g at 0.5 A/g	2E	10000	88.4 % at 5 A/g	42.1	KOH	1.6	
$CuCo_2O_4$/CuO	57 F/g at 1 mA/cm²	2E (vs. AC)	5000	79% at 5 mA/cm²	18	KOH	1.5	S8 (2016)
$CuCo_2O_4$ nanostructures	338 F/g at 1 A/g	3E	-	-	-	KOH	0.5	S9 (2014)
$FeCo_2O_4$ tube arrays	0.67 F/cm² at 2 mA/cm²	2E (sym)	2000	94 % at 4 mA/cm²	30.9	KOH	1	S10 (2016)
$NiCo_2S_4$@$NiCo_2S_4$ nanosheets	4.38 F/cm² at 5 mA/cm²	3E	5000	82% at 30 mA/cm²	-	KOH	0.55	S11 (2015)
	75 F/g at 5 mA/cm²	2E (vs.RGO)	5000	81% at 20 mA/cm²	24.9	KOH	1.55	
$NiCo_2S_4$@Ni-Mn LDH/GS	1.74 F/cm² at 1 mA/cm²	3E	1000	88.3 % at 5 mA/cm²	-	KOH	0.5	S12 (2015)
	0.5 F/cm² at 5 mA/cm²	2E (vs. VN)	5000	84.5 % at 20 mA/cm²	-	KOH	1.5	
$NiCo_2S_4$@MnO_2 core/shell	2.6 F/cm² at 3 mA/cm²	3E	5000	104 % at 50 mV/s	-	KOH	0.55	S13 (2015)
$NiCo_2S_4$@MnO_2 heterostructures	1338 F/g at 2 A/g	3E	2000	82 % at 10 A/g	-	KOH	0.45	S14 (2015)

$ZnCo_2O_4$ nanowires on carbon textile	1283 F/g at 1 A/g	3E	5000	Negligible at 8 A/g	-	KOH	0.4	S15 (2014)
nickel cobalt oxide nanowires	1479 F/g at 1 A/g	3E	-	-	-	KOH	0.5	S16 (2014)
	105 F/g at 3.6 mA/cm^2	2E(vs. AC)	3000	83 % at 20 mV/s	37.4	KOH	1.6	
Co_3O_4@PPy@MnO_2 nanowires	629 F/g at 1.2 mA/cm^2	3E	-	-	-	KOH	0.8	S17 (2014)
	96.5 F/g at 0.1 A/g	2E (vs. AC)	10000	100 % at 3 A/g	34.3	KOH	1.6	
$ZnCo_2O_4$ nanowire	1625 F/g at 5 A/g	3E	5000	94 % at 20 A/g	-	KOH	0.5	S18 (2014)
	0.34 F/cm^2 at 1 mA/cm^2	2E (Symm)	-	-	12.5	KOH	0.8	
$ZnCo_2O_4$ nanoflakes	1220 F/g at 2 A/g	3E	5000	94.2 % at 2 A/g	-	KOH	0.6	S19 (2015)
CeO_2@MnO_2 core-shell	255 F/g at 0.25 A/g	3E	3000	90.1 % at 2 A/g	-	Na_2SO_4	0.8	S20 (2015)
	49.5 F/g at 0.25 A/g	2E (vs. AGO)	-	-	25.7	Na_2SO_4	2	
$ZnCo_2O_4$@MnO_2 core-shell	2.4 F/cm^2 at 6 mA/cm^2	3E	5000	90% at 24 mA/cm^2	-	KOH	0.5	S21 (2015)
	0.4 F/cm^2 at 2.5 mA/cm^2	2E (Fe2O3)	5000	91% at 5 mA/cm^2	37.8	KOH	1.3	
$NiCo_2S_4$ Nanotube on carbon fiber paper	2.86 F/cm^2 at 4 mA/cm^2	3E	2000	96 % at 10 mA/cm^2	-	KOH	0.5	S22 (2014)
Zn-Ni-Co ternary oxide	4.2 F/cm^2 at 1.7 mA/cm^2	3E	6000	80.9 % at 10 A/g	-	KOH	0.5	S23 (2015)
	114 F/g at 1 A/g	2E (vs. AC)	6000	71.2 % at 3 A/g	35.6	KOH	1.5	
$NiCo_2O_4$@$NiMoO_4$ nanowires	1067 F/g at 10 mA/cm^2	3E	5000	84 % at 10 mA/cm^2	-	KOH	0.5	S24 (2015)
	-	2E (vs. AC)	5000	87 % at 10 mA/cm^2	-	KOH	1.4	
nickel copper oxide nanowires	2.24 F/cm^2 at 10 mA	3E	1000	90 % at 10 A/g	-	KOH	0.5	S25 (2014)
	126 F/g at 2 mA/cm^2	2E (vs. AC)	5000	87 % at 20 mA/cm^2	30	KOH	1.3	
Al@Ni@MnO_x nanospike	942 F/g at 50 mV/s	3E	-	-	-	Na_2SO_4	0.8	S26 (2015)
	59 F/g at 10 mV/s	2E (vs. CCG)	1100	96.3 % at 2 A/g	23.02	PVA/Na_2SO_4	1.8	
Carbon fiber paper@ $NiCo_2O_4$ nanowires	680 F/g at 0.5 A/g	3E	-	-	-	NaOH	0.45	S27 (2015)
	97.5 F/g at 1 A/g	2E (vs. GF)	10000	92.2 % at 2 A/g	34.5	NaOH	1.6	
DS-$CuCo_2O_4$	**1472 F/g (2.94 F/cm^2) at 4 mA/cm^2**	**3E**	**5000**	**93.8 % at 10 mA/cm^2**	**-**	**KOH**	**0.5**	**This work**
	119 F/g (1.19 F/cm^2) at 20 mA/cm^2	**2E (vs. AC)**	**6000**	**92.5 % at 50 mA/cm^2**	**37.3**	**KOH**	**1.5**	

S1. Q. Wang, D. Chen and D. Zhang, *RSC Adv.*, 2015, **5**, 96448.
S2. J. Cheng, H. Yan, Y. Lu, K. Qiu, X. Hou, J. Xu, L. Han, X. Liu, J.-K. Kim and Y. Luo, *J. Mater. Chem. A*, 2015, **3**, 9769.
S3. S. Vijayakumar, S.-H. Lee and K.-S. Ryu, *Electrochim. Acta*, 2015, **182**, 979.
S4. M. Kuang, X. Y. Liu, F. Dong and Y. X. Zhang, *J. Mater. Chem. A*, 2015, **3**, 21528.
S5. Q. Wang , J. Xu, X. Wang, B. Liu, X. Hou, G. Yu, P. Wang, D. Chen and G. Shen, *ChemElectroChem*, 2014, **1**, 559.
S6. K. Zhang, W. Zeng, G. Zhang, S. Hou, F. Wang, T. Wang and H. Duan, *RSC Adv.*, 2015, **5**, 69636.
S7. S. Liu, K. San Hui, K. N. Hui, J. M. Yun and K. H. Kim, *J. Mater. Chem. A*, 2016, **4**, 8061.
S8. A. Shanmugavani and R. K. Selvan, *Electrochim. Acta*, 2016, **188**, 852.
S9. A. Pendashteh, M. S. Rahmanifar, R. B. Kaner and M. F. Mousavi, *Chem. Commun.,* 2014, **50**, 1972.
S10. B. Zhu, S. Tang, S. Vongehr, H. Xie, J. Zhu and X. Meng, *Chem. Commun.*, 2016, **52**, 2624.
S11. H. Chen, S. Chen, H. Shao, C. Li, M. Fan, D. Chen, G. Tian and K. Shu, *Chem. Asian J.*, 2015, **11**, 248.
S12. H. Wan, J. Liu, Y. Ruan, L. Lv, L. Peng, X. Ji, L. Miao and J. Jiang, *ACS appl. mater. interfaces*, 2015, **7**, 15840.
S13. K. Xu, Q. Ren, Q. Liu, W. Li, R. Zou and J. Hu, *RSC Adv.*, 2015, **5**, 44642.
S14. J. Yang, M. Ma, C. Sun, Y. Zhang, W. Huang and X. Dong, *J. Mater. Chem. A*, 2015, **3**, 1258.
S15. L. Shen, Q. Che, H. Li and X. Zhang, *Adv. Funct. Mater.*, 2014, **24**, 2630.
S16. X. Wang, C. Yan, A. Sumboja and P. S. Lee, *Nano Energy*, 2014, **3**, 119.
S17. L. Han, P. Tang and L. Zhang, *Nano Energy*, 2014, **7**, 42.
S18. S. Wang, J. Pu, Y. Tong, Y. Cheng, Y. Gao and Z. Wang, *J. Mater. Chem. A*, 2014, **2**, 5434.
S19. J. Cheng, Y. Lu, K. Qiu, H. Yan, X. Hou, J. Xu, L. Han, X. Liu, J.-K. Kim and Y. Luo, *Phys. Chem. Chem. Phys.*, 2015, **17**, 17016.
S20. S. J. Zhu, J. Q. Jia, T. Wang, D. Zhao, J. Yang, F. Dong, Z. G. Shang and Y. X. Zhang, *Chem. Commun.*, 2015, **51**, 14840.
S21. W. Ma, H. Nan, Z. Gu, B. Geng and X. Zhang, *J. Mater. Chem. A*, 2015, **3**, 5442.
S22. J. Xiao, L. Wan, S. Yang, F. Xiao and S. Wang, *Nano Lett.*, 2014, **14**, 831.
S23. C. Wu, J. Cai, Q. Zhang, X. Zhou, Y. Zhu, P. K. Shen and K. Zhang, *ACS Appl. Mater. Interfaces*, 2015, **7**, 26512.
S24. Z. Gu, H. Nan, B. Geng and X. Zhang, *J. Mater. Chem. A*, 2015, **3**, 12069.
S25. L. Zhang, C. Tang and H. Gong, *Nanoscale*, 2014, **6**, 12981.
S26. J. Yang, G. Li, Z. Pan, M. Liu, Y. Hou, Y. Xu, H. Deng, L. Sheng, X. Zhao, Y. Qiu and Y. Zhang, *ACS appl. mater. interfaces*, 2015, **7**, 22172.
S27. Q. Tang, M. Chen, L. Wang and G. Wang, *J. Power Sources*, 2015, **273**, 654.

References